In-Situ Atomic Level Studies of Gd Atom Release and Migration on Graphene from a Metallofullerene Precursor

Sapna Sinha[1], Yuewen Sheng[1], Ian Griffiths[1], Neil P. Young[1], Si Zhou[1], Angus I. Kirkland[1,2], Kyriakos Porfyrakis[1], Jamie H. Warner[1*]*

[1]Department of Materials, University of Oxford, 16 Parks Road, Oxford, OX1 3PH, United Kingdom

[2]Electron Physical Sciences Imaging Center, Diamond Light Source Ltd, Didcot, OX11 0DE, United Kingdom

Email: *jamie.warner@materials.ox.ac.uk, *kyriakos.porfyrakis@materials.ox.ac.uk

Abstract

We show how Gd based metallofullerene ($Gd_3N@C_{80}$) molecules can be used to create single adatoms and nanoclusters on a graphene surface. An *in-situ* heating holder within an aberration corrected scanning transmission electron microscope is used to track the adhesion of endohedral metallofullerenes (MFs) to the surface of graphene, followed by Gd metal ejection and diffusion across the surface. Heating to 900°C is used to promote adatom migration and metal nanocluster formation, enabling direct imaging of the assembly of nanoclusters of Gd. We show that hydrogen can be used to reduce the temperature of MF fragmentation and metal ejection, enabling Gd nanocluster formation on graphene surfaces at temperatures as low as 300°C. The process of MF fragmentation and metal ejection is captured *in-situ* and reveals that

after metal release, the C_{80} cage opens further and fuses with the surface monolayer carbon glass on graphene, creating a highly stable carbon layer for further Gd adatom adhesion. Small voids and defects (~1nm) in the surface carbon glass act as trapping sites for Gd atoms, leading to atomic self-assembly of 2D monolayer Gd clusters. These results show that MFs can adhere to graphene surfaces at temperatures well above their bulk sublimation point, indicating that the surface bound MFs have strong adhesion to dangling bonds on graphene surfaces. The ability to create dispersed single Gd adatoms, and Gd nanoclusters on graphene may have impact in spintronics and magnetism.

KEYWORDS: ADF-STEM, Gd, graphene, 2D materials, metallofullerenes, TEM

Expanding the properties of 2D materials requires integration with other systems, such as molecules, to provide new functionality and applications.[1–4] In particular, the strong sp^2 bond between carbon atoms in graphene gives an opportunity for adatom adsorption. Decorating the surface of graphene with adatoms and nanoclusters is one approach that can alter the band structure of graphene and introduce dopants that can modify the p-type and n-type behavior.[5] The use of graphene as a highly conductive electrode for applications such as catalysis also requires the integration of metal atoms and nanoparticles on the surface.[6] For spintronic applications or ferromagnetics involving graphene, the introduction of spin-bearing molecular systems that can interact with the high mobility conduction electrons is also crucial.

There are many different approaches for introducing surface dopants to graphene, such as thermal evaporation,[7] chemical vapor deposition,[8,9] e-beam evaporation,[10] solution deposition of molecules/nanoparticles,[11–14] and the direct formation of material from deposited precursors. There have been a wide range of materials investigated as surface dopants and also as substitutional dopants in graphene, such as N, Si , P, B, Fe, Au [15–20] as substitutions, and Co, Pt, Ni, Au, Gd as surface dopants.[5,21–

[23] Importantly, doping can lead to changes in the conductivity, magnetism, transparency, and catalytic response.[6]

Many of these systems have been studied at atomic resolution using transmission electron microscopy (TEM)[24,25] and electron energy loss spectroscopy (EELS). Annular dark field scanning transmission electron microscopy (ADF-STEM) can provide non-linear Z-dependent contrast that helps to discriminate the dopant from the C lattice with higher contrast than phase contrast TEM, however phase contrast TEM enables the dynamics to be observed at much faster time scales. Furthermore the bond lengths between substitutional dopants and C can be accurately measured from phase contrast TEM images, as has been demonstrated in measurements of elongated Si-C bonding at defects and edges of graphene.[26,27] Substitutional N dopants in graphene, typically only replace single C atoms, whereas larger atoms such as Si and Fe can form both single or double substitutions of C in the lattice.[28] EELS has been used to show different oxidation states for Si and Fe atoms as they transition between bonding to either 3 C atoms or 4 C atoms during electron beam induced transformations.[20,29] Larger atoms such as Au are generally found in sites larger than the C monovacancy. However, the formation of stable systems using surface doping of graphene is much more challenging due to the low migration barrier for diffusion of atoms on pristine graphene surfaces.

At room temperature, most atomic species have sufficient thermal energy to overcome the diffusion barrier and migrate freely across pristine graphene until they find either a defect, edge, or surface carbon glass layer. Prior work using *in-situ* heating within an aberration corrected TEM showed that Au nanocrystals form 2D monolayer and bilayer structures at high temperatures of 500-800^{o}C, and attach to defects and the edges of holes in graphene.[22] The observation of crystalline Au significantly above its predicted melting point indicated that surface interactions with graphene can lead to modified melting and

evaporation behaviour. Recent work has shown that 2D Pt monolayers can be found across in pristine graphene regions, formed by electrochemical deposition methods,[30] but it is likely that these 2D Pt layers are initially nucleated from the binding of Pt atoms to the edge of surface carbon glass and then extend lateral out into the pristine regions. This is also because the diffusion of Pt on graphene has a low energy barrier which cannot lead to Pt atomic localization in pristine graphene regions.

The deposition of most materials onto a graphene surface generally leads to them adhering to the surface carbon glass, which has sp^2 character but with heavy defect density of pentagons and heptagons, and also contains elements such as N and O.[31] In graphene grown by chemical vapour deposition (CVD), Si atoms are commonly found attached to this surface carbon glass. Recent work on understanding the interactions between Pt single atoms and MoS_2 monolayers also showed that Pt atoms only adhere to this surface carbon glass or to S vacancies in the MoS_2, with the diffusion across pristine MoS_2 having a low energy barrier.[32] In some cases, the presence of metal atoms on the surface of graphene causes catalytically promoted etching of the graphene, which leads to hole formation. Such effects are generally detrimental to the formation of well-ordered graphene-dopant systems. Studying the interactions between precursors, their reactive elements and graphene at the atomic scale is therefore important for the development of new 2D layered systems beyond graphene. One of the least damaging way of achieving molecular doping of graphene is by introducing organic and inorganic molecules to the graphene surface as carriers of the dopants, which can later self-assemble and decompose when heated. Similar approaches have been applied for many years to the interior of carbon nanotubes, where numerous materials were used to fill the inner void of single walled and multi-walled carbon nanotubes and the resulting chemical reactions investigated.[33–35] For graphene, few studies have been carried out on rare-earth magnetic particles and this field has yet to be fully explored for a diverse range of materials compared to those studied in nanotubes.

An understanding of metal adsorption and interaction with graphene is however, vital to the development of electronic devices based on this material.

In this work, we study the interaction of metallofullerenes (MFs) containing Gadolinium metal, a rare earth element, with the surface of graphene. Gd dopants show magnetic and spin properties that may yield interesting composite systems for spintronic applications. Theoretical calculations have shown that the Gd adatoms can significantly enhance the magnetic moment of graphene.[21,36] In addition, the sign and magnitude of magnetic anisotropy of such Gd-graphene hybrid was found to be based on the carrier accumulation.[37] The deposition of Gd onto graphene has been shown to result in n-type doping,[38] which is important as graphene is often p-type doped from interactions with substrates, water and surface residues.

Herein, we investigate the atomic scale interactions between Gd atoms and graphene by the use of a Gd containing molecular precursor, in the form of high purity $Gd_3N@C_{80}$ (see experimental section) for metal cargo release to achieve single Gd adatom dopants and clusters on the surface of graphene. An *in-situ* heating holder is used to heat the MF-graphene film stepwise to 900^{o}C, with atomic resolution tracking using TEM of the structural transformation pathways. This was carried out by using FIB to cut slits into a SiN heating chip and transferring graphene suspended across the slit. *Ex-situ* experiments are performed using hydrogen to achieve MF cage rupture at low temperatures and subsequent Gd atom decoration across monolayer graphene surfaces. Hydrogen is known to induce cage fragmentation[39] and offers a means to achieve chemical reactions between MFs and graphene surfaces at much lower temperatures than thermal annealing alone. ADF-STEM is used at both 60kV for *in-situ* heating work, and at 200kV for room temperature imaging. The higher accelerating voltage enables visualization of the Gd metal without the significant contrast from beam induced contamination at room temperature that occurs at lower voltages.

The high atomic number of Gd enables easy identification in the presence of carbon atoms, surface carbon residue, and other lighter inorganic contaminants that are known to exist within graphene grown by chemical vapour deposition. Longer time-lapse studies and higher temperature studies have been carried out using ADF-STEM at 60kV to avoid damage of the graphene.[40,41]

Results and discussion

Figure 1a-c shows a schematic illustration of MF deposition onto graphene. Two types of TEM grids were used, one for ex-situ work (SiN with 2 micron holes), the other being SiN *in-situ* heating chips with FIB cut slits. Graphene grown by CVD was transferred onto the TEM grids to give suspended areas suitable for ADF-STEM imaging. The graphene samples were cleaned after transfer by annealing to remove excess PMMA resist residue. The MFs were drop cast onto the TEM chips from a CS_2 solution and allowed to dry. CS_2 is a good solvent for endohedral metallofullerenes (MFs) and also has a high volatility, leaving minimal surface adsorbates on graphene. Some ex-situ samples were then annealed in argon/hydrogen gas after the MF deposition at 180^{o}C to promote MF-graphene chemical reactions. Initial attempts to image MFs on the surface of graphene using ADF-STEM at room temperature at 60kV were limited by excessive beam induced contamination. Therefore imaging at 200kV was used, as the dynamics of MFs could be studied within a short window of time before beam induced damage occurred and beam induced contamination was less limiting due to the lower contrast from light Z elements that are typical within the contamination. Figure 1(d) shows a low magnification optical image of the $Gd_3N@C_{80}$–graphene hybrid system on a SiN chip and Figure 1(e) shows a typical selected area electron diffraction pattern from the suspended graphene regions. Figure 1f shows a low magnification TEM image of graphene with surface bound MFs, with an energy dispersive x-ray (EDX) spectrum was taken from the red boxed area, shown in figure 1g. The EDX spectrum of the hybrid sample shows the presence of

Gadolinium atoms together with silicon and copper peaks from the impurities from the SiN substrate and copper substrate used during typical CVD synthesis of graphene, respectively.

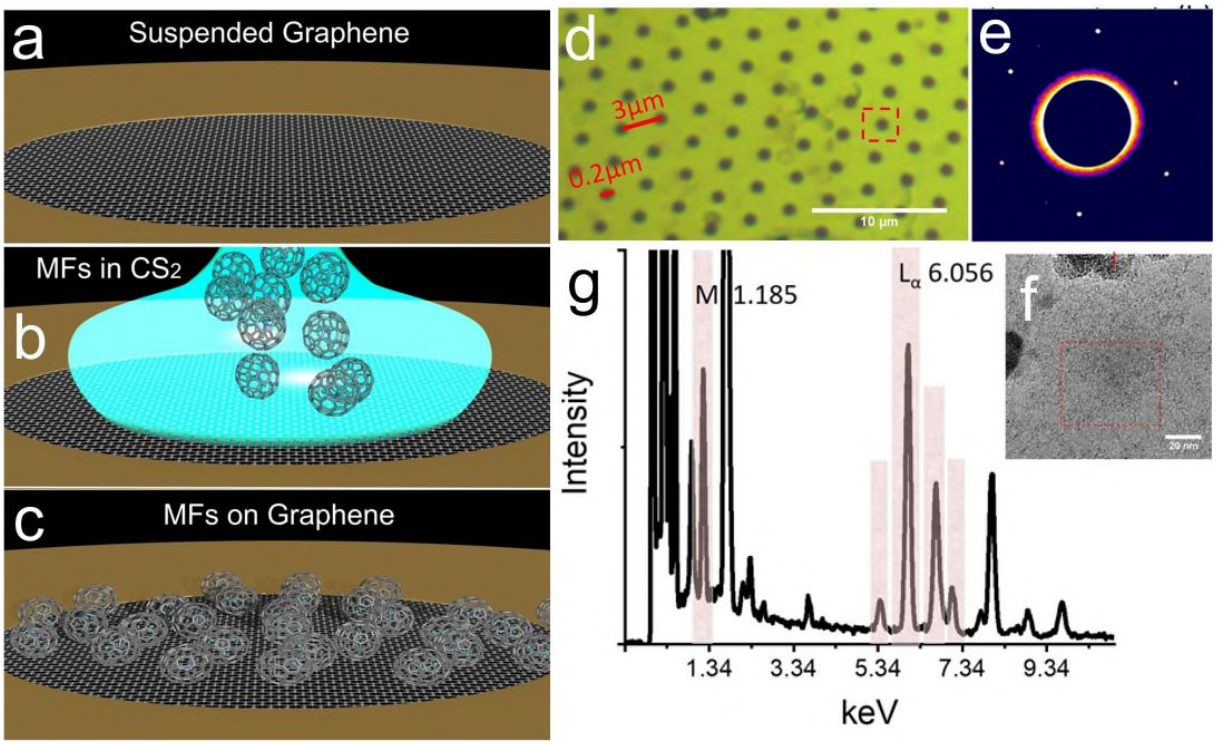

Figure 1. (a)-(c) Schematic illustration showing the deposition of MFs from solution onto the surface of graphene on a TEM grid. (d) Optical image showing the SiN TEM grid with graphene suspended across the holes. (e) Selected area electron diffraction pattern from an area of graphene suspended across the hole. (f) Low magnification TEM image of graphene with surface bound MFs indicating the region where EDX spectrum was recorded. (g) EDX spectrum from the red boxed region in (f) with Gd M and Lα peaks indicated and other L peaks highlighted.

Figure 2 (a) shows an ADF-STEM image recorded using an accelerating voltage of 200kV of isolated $Gd_3N@C_{80}$ molecules dispersed on graphene, with metal trimer clusters clearly visible (figure 2b). In general, the MFs were well dispersed across the graphene surface, mostly with sub-monolayer density, but some areas showed denser clusters of MFs, as expected from a drop-cast solution preparation. The projection of the three Gd atoms show variability, indicating they are randomly orientated across the surface. ADF-STEM image simulations were calculated using the multislice method,[42,43] from the atomic

model shown in figure 2c,d, for random orientations to show the effect on the relative Gd locations (figure 2e). The green box in figure 2e shows the case when the orientation of the MF is such that two Gd atoms overlap in projection, giving rise to only two spots, with one of increased intensity relative to the other. The yellow box in figure 2e shows the case when the orientation leads to a linear projection of the three Gd atoms in the MF with equal intensity. The red box in figure 2e shows the case when the orientation of the Gd trimer is parallel to the graphene lattice giving rise to a symmetric triangular intensity pattern (figure 2f). When noise was added to this image simulation, figure 2g, it showed good qualitative agreement with the experimental ADF-STEM image (figure 2h).

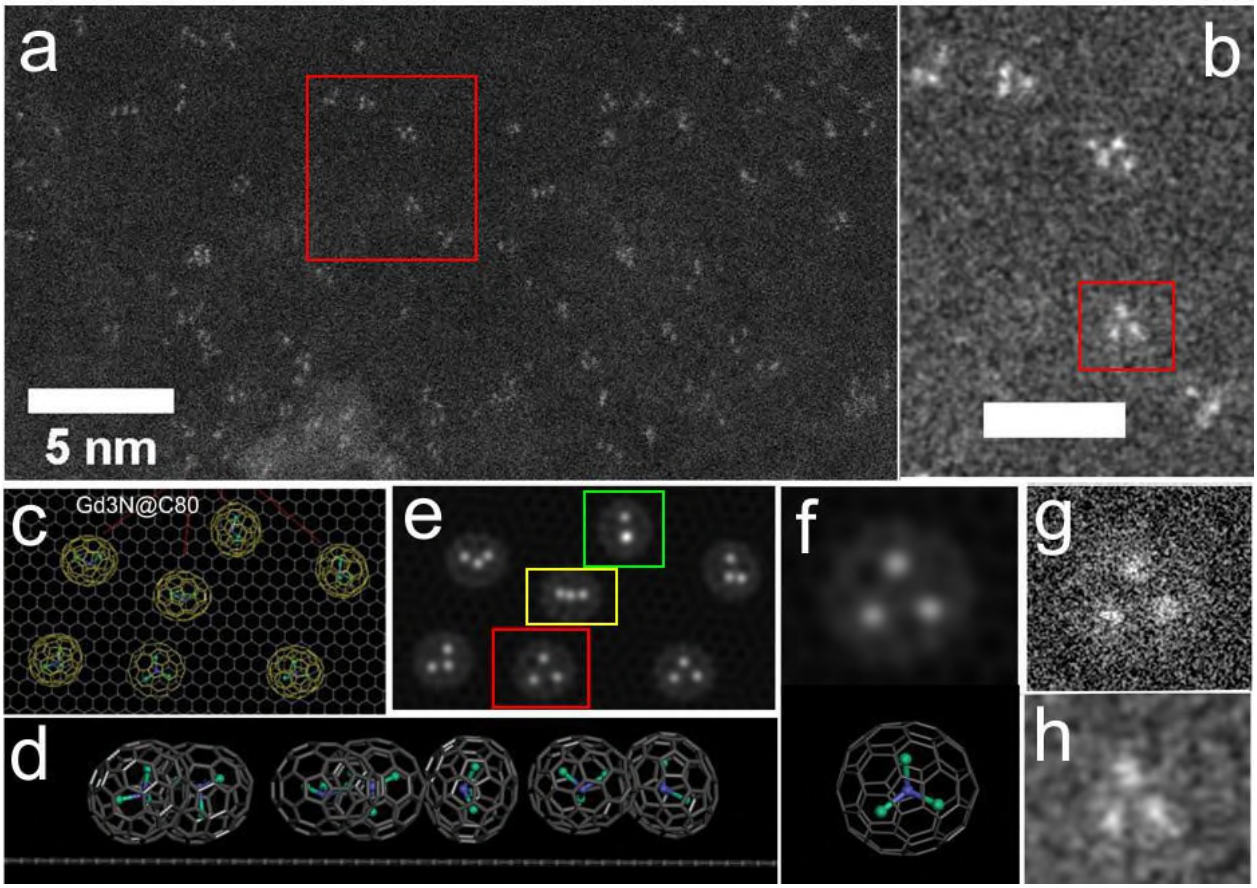

Figure 2. (a) Room temperature 200kV ADF-STEM imaging of isolated $Gd_3N@C_{80}$ molecules on graphene. (b) Higher magnification image of the red boxed region in (a) showing several trimer contrast features from MFs. (c) Atomic model of $Gd_3N@C_{80}$ molecules on the surface of graphene (top view), and (d) side view. (e) Multislice

ADF-STEM image simulation of the atomic model in (c) showing intensities from the Gd metal trimer atoms in various projected orientations. (f) Comparison of the image simulation from the red box area in (e) with the atomic model. (g) Noise added to the ADF-STEM simulated image in (f) compared to the experimental image shown in (h), taken from the red boxed region in (b).

Time series of images (figure 3a-e), revealed that the MFs showed both translational motion (green line in figure 3a-e), as well as rotational dynamics, figure 3f-y. Figure 3f-j shows a magnified view of the red boxed region indicated in figure 3a. This region contains two adjacent MFs, with changes to the Gd trimer intensities from frame to frame (figure 3f-j). Multi-slice image simulations, with added noise, shown in figure 3k-o, are based on the atomic models shown in figure 3p-t, and qualitatively match the experimental intensity profiles. Figure 3f-j, together with the image simulations shown in figure 3k-o, show that the MFs are rotating and also moving apart. The orientation of the Gd trimer is indicated in figure 3u-y, where the fullerene cages have been removed for visual clarity. It is known that the Gd_3N cluster within a C_{80} cage does not have completely free rotation at room temperature [44,45], and prior reports of C_{60} within graphene sandwiches showed dynamic translational motion together with fullerenes on the surface of graphene that migrate [46]. MFs trapped within peapods also exhibit rotation and translation motion of the entire molecule. This indicates that it is most likely that the entire MF molecule is rotating on the surface of graphene, rather than the Gd trimer rotating within a stationary MF.

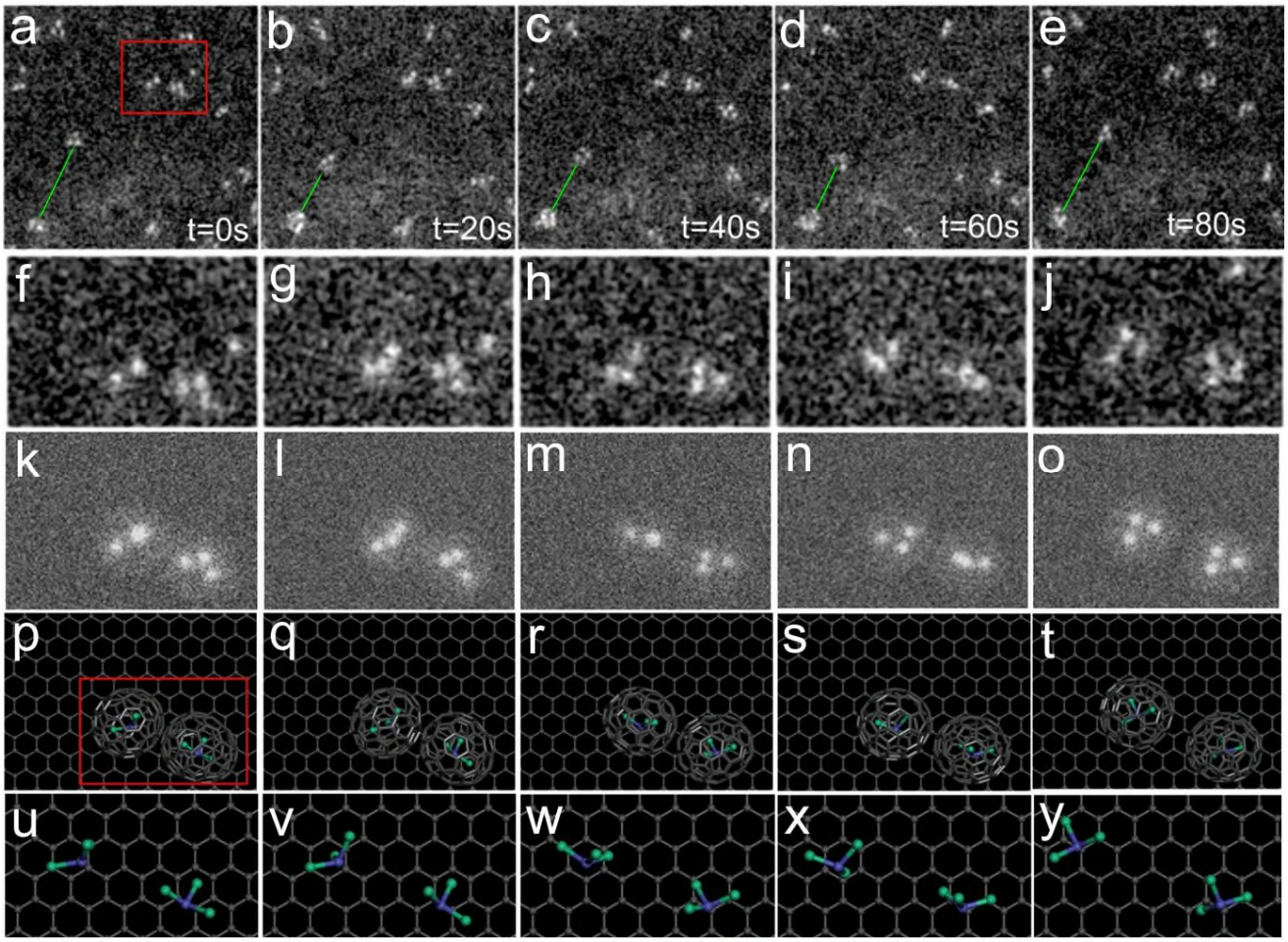

Figure 3. (a)-(e) Time series of ADF-STEM images recorded at 200kV, 20 s apart, showing trimer dynamics. The green line indicates translation migration of one MF relative to another. Magnified views are shown in (f)-(j) from the red boxed region indicated in (a). (k)-(o) Multi-slice ADF STEM image simulations with added noise based on the atomic models shown in (p)-(t). (u)-(y). Enlargement of the red boxed area in (p), with the fullerene cage removed to reveal the relative orientations of the Gd trimer.

To further explore the behavior of MFs on graphene surface, we utilized *in-situ* heating to provide thermal energy to initiate chemical reactions. This also has the benefit that beam induced contamination is significantly reduced at higher temperatures. Our first set of observations were made at 300^{o}C, where

several MF molecules were observed isolated and immobilized on the graphene surface (figure 4). Figure 4a shows a low magnification ADF-STEM image of monolayer graphene on the *in-situ* heating TEM chip with deposited $Gd_3N@C_{80}$ at 300ºC. The weak intensity visible is indicative of the surface coating of the MFs on graphene before high temperature is reached. Figure 4b shows a higher magnification ADF-STEM image of the sample after heating to 500ºC *in-situ*. Large sections of clean graphene are visible, along with a thin surface carbon layer and bright intensity from Gd atoms in both clusters and as isolated MFs. The higher magnification ADF-STEM image in figure 4d clearly shows this, with yellow circles indicating immobilized $Gd_3N@C_{80}$ MFs attached to the surface carbon layer. Some other impurity atoms are also present showing intensities that are higher than those from carbon but less than the heavy Gd; most likely these are Si atoms that are known to be contaminants in graphene samples grown by CVD. The MF circled in red within the red boxed region in figure 4c is shown in more detail in figure 4d and 4e. The Gd trimer is clearly visible in figure 4d,e, along with diffuse intensity from the fullerene cage. The MF is attached to the side of the surface carbon layer, and sits on top of graphene. The power spectrum inset to figure 4d shows the hexagonal reflections associated with monolayer graphene. The yellow box in figure 4d shows an empty fullerene cage after Gd atoms have been released. The Gd-Gd spacing was measured from figure 4e, using line profiles, showing an average Gd-Gd distance of 0.34+/-0.02nm, which is in excellent agreement with the known Gd-Gd distance in $Gd_3N@C_{80}$.[44] Since the molecules have different orientation, the error in distance measurement comes from the degree of rotation. The line profile analysis in figure 4f shows increased intensity at the edges of the MF confirming the spherical nature of the object, rather than a flat disk which would have uniform contrast profile.

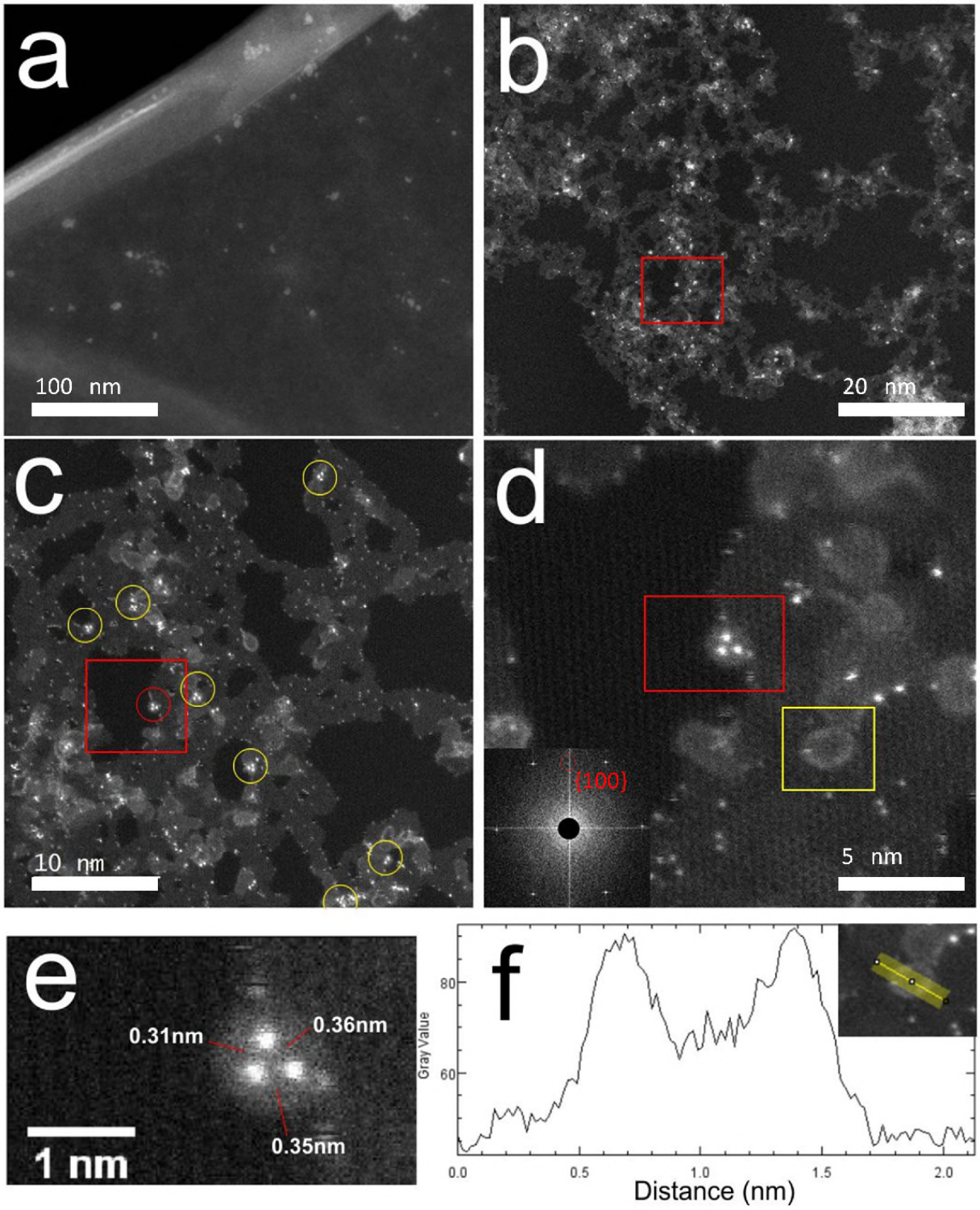

Figure 4. *In-situ* ADF-STEM images of $Gd_3N@C_{80}$ on graphene recorded at 60kV. (a) Low magnification ADF-STEM image of graphene suspended on an *in-situ* heating TEM grid with deposited MFs. Temperature is 300°C.

(b) ADF-STEM image at 500°C showing graphene with surface material. (c) ADF-STEM image from the red boxed area in (b) showing clean pristine patches of graphene along with a thin surface layer of carbon glass, with individual MFs attached, indicated by the yellow circles. (d) ADF-STEM image from the red boxed region in (c) showing a single $Gd_3N@C_{80}$ attached to the edge of the surface carbon glass. Inset shows the power spectrum indicating that monolayer graphene supports this region. The red boxed area shows the single MF and the yellow boxed area shows an empty fullerene cage attached to the surface. (e) ADF-STEM image from the red boxed area in (d) showing a single $Gd_3N@C_{80}$. Distances between Gd atoms are indicated. (f) Line profile taken across the empty fullerene cage, from the yellow boxed area in (d), showing increased intensity at the edge that is typical for fullerene cage. Inset shows the location of the line profile. *In-situ* temperatures are: (a) 300°C, (b)-(f) 500°C

Figure 5 shows a series of ADF-STEM images recorded at 500°C that capture the metal cargo release onto the carbon glass and subsequent decomposition of the C_{82} cage, followed by its fusion with the surface monolayer carbon glass. This process is driven *in-situ* by the combined result of heating and high energy electron beam induced effects. The transformation occurs sufficiently slowly to capture the fullerene cage opening. Multislice image simulations were used to help understand the expected intensities from the decomposing and fusing MFs, figure 5f-j, based on schematic atomic models shown in figure 5k-o. After breaking the C_{82} cage, the pyramidal structure of the Gd_3N trimer[47] becomes energetically unstable, leading to the breaking of the Gd-N bonds and single atom Gd atoms diffusing across the carbon glass, figure 5d,e or migrating across the edges (S.I. 1). The schematic atomic models in figure 5p-r illustrate the process where $Gd_3N@C_{80}$ is first immobilized by attachment to the edge of the existing surface carbon layer on top of graphene (figure 5p) followed by cage opening (figure 5q). After Gd metal release the cage fuses with the surface carbon to enlarge its area (figure 5r). This suggests that the surface carbon layer present in the sample also contains material from other fused fullerene cages to form this monolayer carbon glass, which is ideal for adhesion of Gd atoms due to its amorphous nature. Gd atoms

are typically seen attached to either the edge of this surface layer, or to defective regions on the surface (figure 5e).

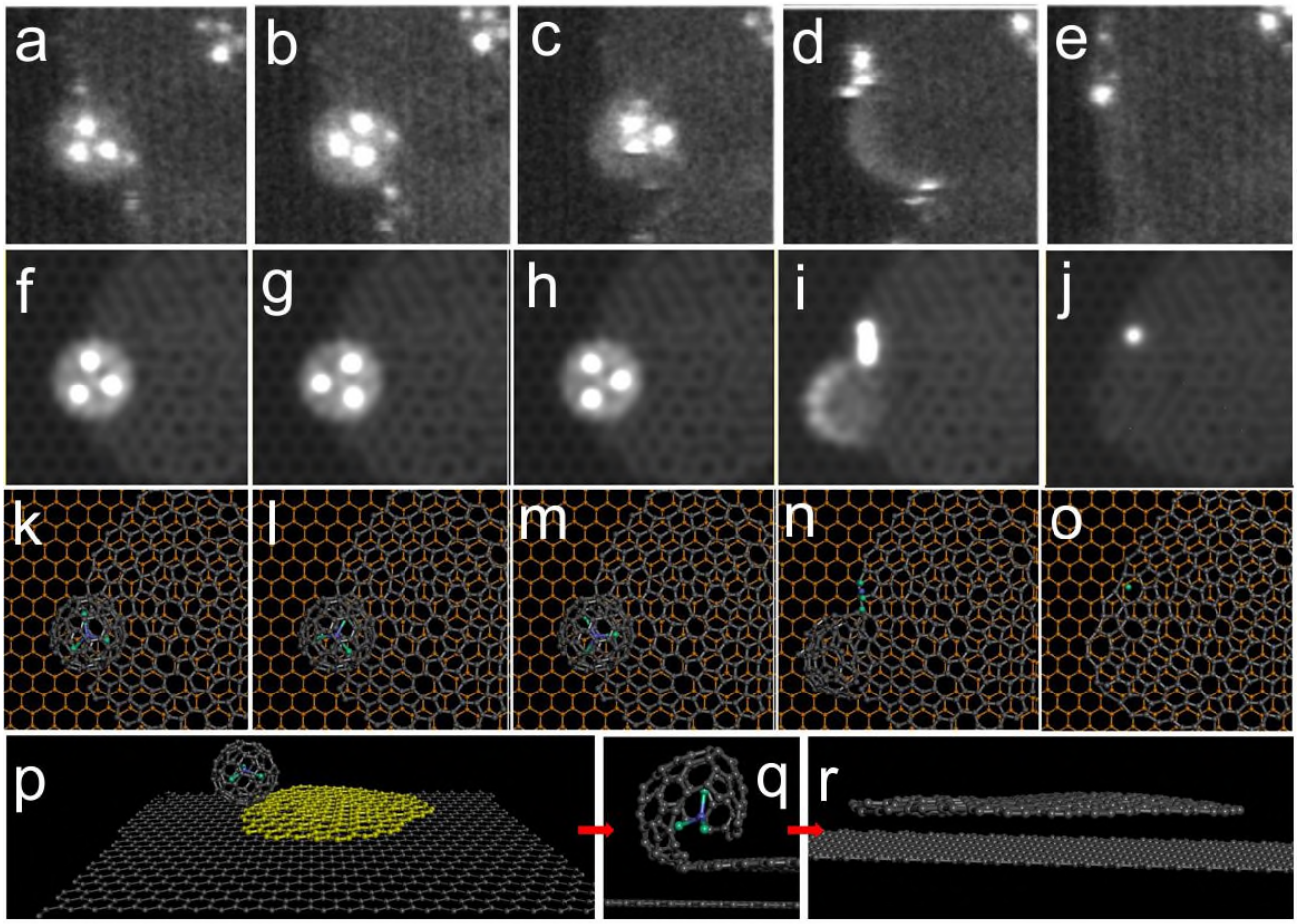

Figure 5. (a)-(e) Time series of ADF-STEM images showing an individual $Gd_3N@C_{80}$ attached to the side of surface carbon layer which fuses, with the release of Gd atoms. Temperature is 500°C; 60kV accelerating voltage. Time between images ~20s. (f)-(j) Multislice image simulations based on the atomic models in (k)-(o), schematically illustrating $Gd_3N@C_{80}$ fusion and Gd atomic release from the cage. (p) 3D schematic model showing a $Gd_3N@C_{80}$ attached to patch of surface carbon (yellow) on graphene. (q) Side view of a schematic atomic model showing cage rupturing and fusion to the surface carbon. (r) 3D Schematic model showing how the cage fusion into the surface carbon layer causes the expansion of the surface region.

In-situ dynamics of Gd atom migration is shown in figure 6, from the region around the yellow box in figure 4d. This area contains a thin monolayer of surface carbon on graphene with three empty fullerenes attached to a small central region of a thicker carbon layer, the empty fullerenes indicated with yellow circles in figure 6a, and six individual Gd atoms indicated with red circles and numbers in figure 6a. The Gd atoms are clearly mobile, with the yellow spot in figure 6b indicating the position jump. The green shaded area shows the underlying monolayer graphene. Gd atoms 1-3 remain localized throughout the sequence, whereas Gd atoms 4-6 are highly active and by figure 6h, these have aggregated into a small cluster on the surface region, away from an edge site. The empty fullerene cage on the right in figure 6a, hosting Gd atom 6, exhibits rotation between frame (a) and (b), which is shown at higher magnification in figure 6i,j. The fullerene appears to have one part anchored to the edge of the central surface carbon material and rotates anti-clockwise. In many cases empty fullerene cages are also observed to migrate and move around the sample. Between figure 6d and e, the fullerene actually detaches and migrates to the right leaving a vacant area where the single Gd atom 6 is now bound to the surface carbon layer. The Gd atom 6 is most likely bonded within the carbon layer, immobilizing it and subsequently Gd atoms 4 and 5 migrate to join it, forming the trimer cluster, shown in detail in figure 6k. The trimer cluster has Gd-Gd distances that are shorter than the Gd-Gd distances observed within the original $Gd_3N@C_{80}$, due to the presence of N in the trimer core of the MF leading to larger bond distances,[44] figure 6l.

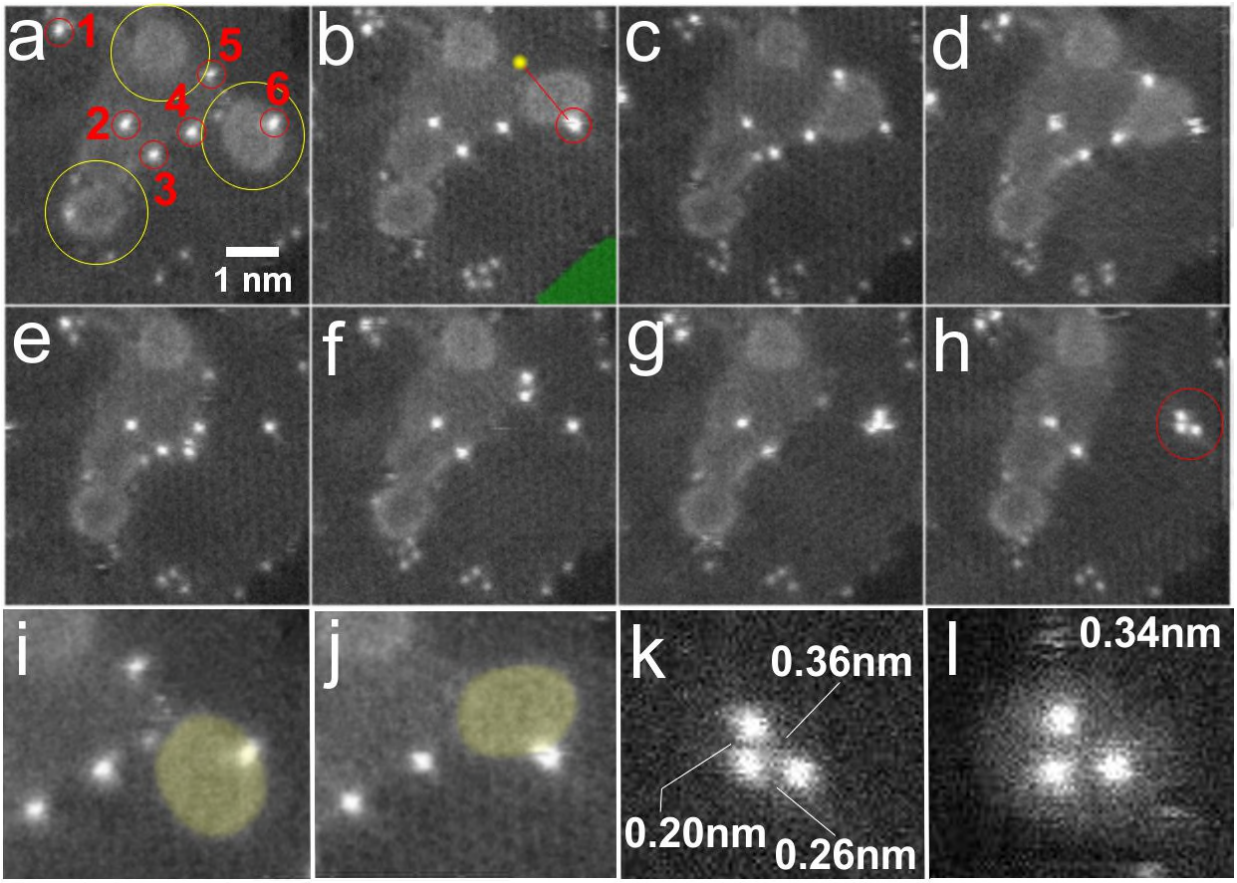

Figure 6. (a)-(h) Time series of *in-situ* ADF-STEM images recorded at 500°C and 60kV accelerating voltage showing migration of single Gd atoms (red circles and numbers in (a)) and movement of empty cages (yellow circle in (a)) on the surface carbon layer on graphene. The green area in (b) indicates a monolayer graphene region. The yellow spot and red line in (b) indicates the initial movement of a Gd atom from the prior frame. Time between frames is 20s. (i)-(j) Magnified views from (a) and (b) of the righthand fullerene cage. Yellow shading indicates the fullerene cage. (k) Magnified view of the Gd cluster indicated by the red circle in (h), with Gd-Gd distances determined from a line profile analysis. (l) ADF-STEM image of a $Gd_3N@C_{80}$ showing a Gd trimer for comparison with the Gd cluster in (k). Distance indicates the average Gd-Gd value.

The data from *in-situ* experiments shown in figures 4-6 were generally carried out at 500°C, above the sublimation point of the MFs (~350°C under high vacuum conditions) and therefore there only a small

density of MFs were found on the surface. In order to explore the activation of Gd atom release from MFs onto graphene surfaces at lower temperatures below the sublimation temperature we used annealing in hydrogen gas at a temperature of 300ºC. The aim of this was to enable a higher density of Gd decoration on the graphene surface. Talyzin *et. al.* studied C_{60}, showing that an increased hydrogenation period results in the fragmentation of the hydrogenated fullerenes following a CH_2 loss pathway.[39] We believe that similar reaction should be active for higher fullerene cages leading to cage opening and thus release of the Gd atoms onto the surface of graphene. Figure 7 shows ADF-STEM images of graphene:$Gd_3N@C_{80}$ samples on *in-situ* heating TEM chips that had been treated under hydrogen for 12 hrs. *In-situ* ADF-STEM imaging was carried out at 300ºC to prevent beam induced contamination. Figure 7a shows bright intensity features on the graphene region, distinctly different to the diffuse appearance seen in samples not treated with hydrogen annealing (figure 4a). Higher magnification ADF-STEM images, figure 7b-e, show that this area consists of Gd nanoclusters that formed on the surface, and that the surface of graphene is also covered with a carbon layer. In this area the Gd concentration appeared high and thus it contained some of the largest Gd clusters observed that were typically 2-4 nm wide and ranging from 1-3 atomic layers of Gd, as estimated from intensity profiles. Figure 7e shows a 2.5nm Gd nanocluster that is predominantly one atom thick, but with some secondary Gd atoms on top. The inset shows a colour version of the ADF-STEM image of the nanocluster showing two levels of intensity, one for single Gd atoms and the other where it is two Gd atoms thick. This is confirmed by line profile analysis comparing the nanocluster to an isolated Gd atom (figure 7f). We did not observe intact $Gd_3N@C_{80}$ MFs on the surface, due to their decomposition and furthermore most of the fullerene cages were fused within the surface carbon layer on graphene.

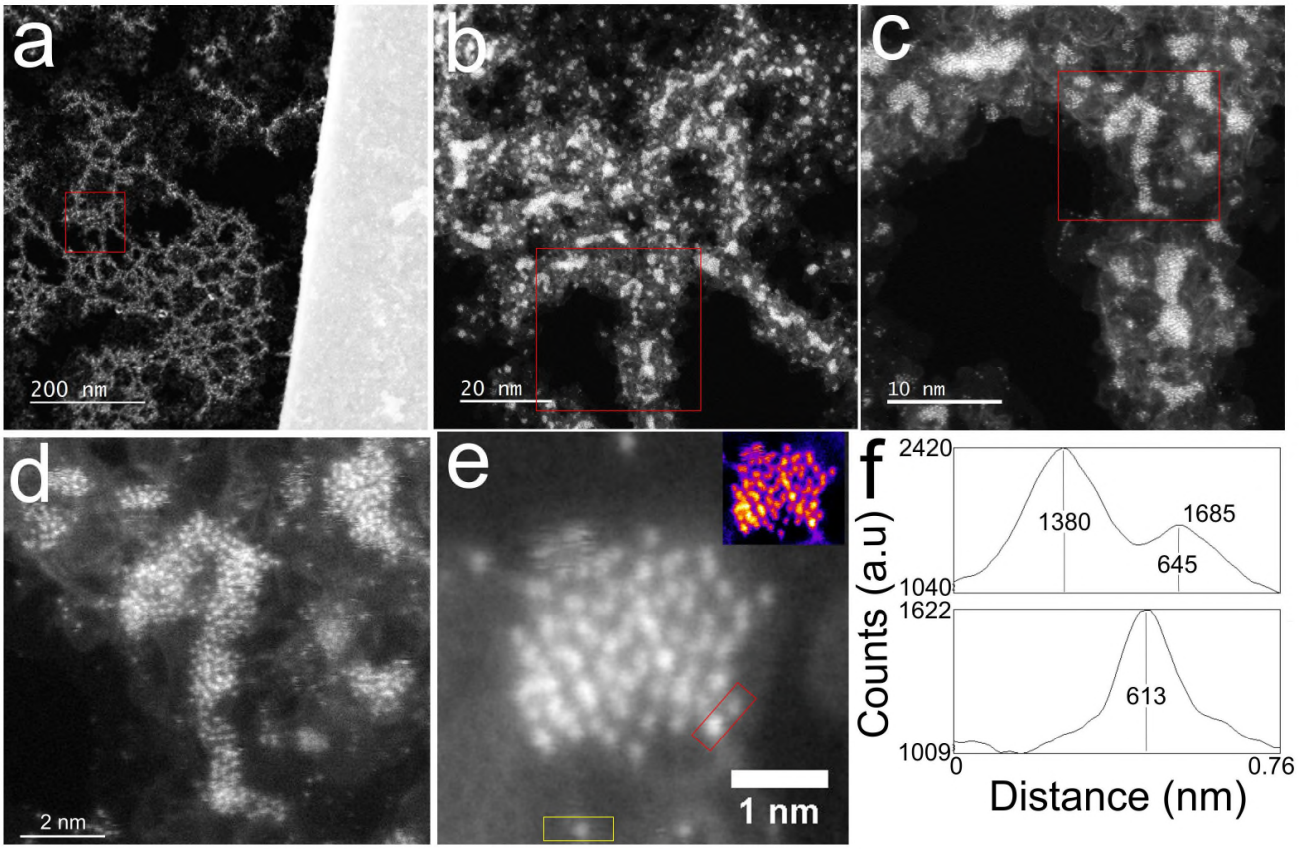

Figure 7. Low magnification ADF-STEM image of graphene:$Gd_3N@C_{80}$ after hydrogen annealing on an *in-situ* SiN TEM chip. The SiN area is on the right. The temperature is 300°C images were recorded at 60kV. (b) Higher magnification ADF-STEM image taken from the red box area in (a). (c) Higher magnification ADF-STEM image taken from the red box area in (b). (d) Higher magnification ADF-STEM image taken from the red box area in (c). (e) ADF-STEM image of a typical Gd nanocluster on the surface of graphene. The inset shows a colour version of the nanocluster to highlight the difference in intensity between single Gd atoms and regions with two Gd atoms in projection. A band pass filter with 100-1 pixel range was applied to the power spectrum to remove the long range intensity variations. (f) Line profiles taken from regions marked by the red box (top) and yellow box (bottom) in (f).

Apart from the high density area shown in figure 7, the majority of the sample contained smaller 1-2nm Gd clusters (figure 8), most likely from an area having initial lower $Gd_3N@C_{80}$ concentration

before hydrogen annealing. Figure 8c shows small Gd clusters containing typically 10-20 Gd atoms, and figure 8d shows a spherical fullerene-like feature that is located within the surface carbon region on graphene. There are also regions of the sample that have even lower Gd concentration (figure 8e), and have isolated Gd atoms and small dimers and few atom clusters.

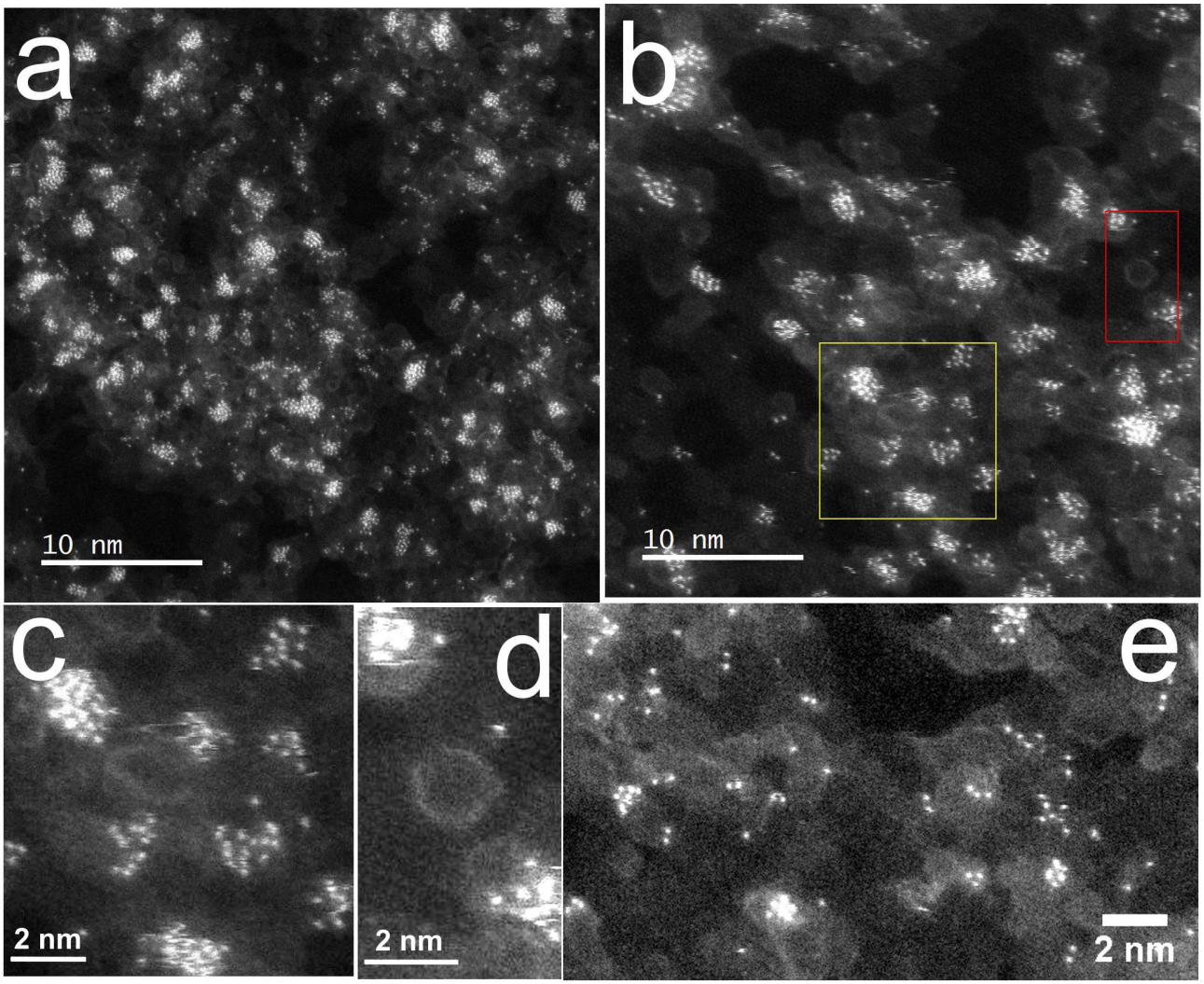

Figure 8. (a) ADF-STEM image of graphene:$Gd_3N@C_{80}$ after hydrogen annealing on an *in-situ* SiN TEM chip. The temperature is 300°C and images were recorded at 60kV. Image taken from an area of lower Gd concentration. (b) ADF-STEM image taken at higher magnification showing 1-2nm Gd clusters on the surface of graphene, along with a visible surface carbon layer that has spherical intensity features. (c) Higher magnification of the region indicated with the yellow box in (b) showing small Gd clusters. (d) Higher magnification image taken from the red

boxed region in (b) showing a fullerene-like feature in the carbon material on graphene. (e) ADF-STEM image from a low Gd concentration region showing many single Gd atom dispersions and small dimer and few atom clusters.

To accelerate the Gd atom diffusion dynamics, we increased the temperature of the *in-situ* chip to 900°C (figure 9). During the *in-situ* heating process from 300°C to 900°C, we observed increased migration rates of Gd atoms allowing the study of Gd atom dynamics and cluster formation. Figure 9 shows a time series of ADF-STEM images of cluster formation from Gd atoms at 900°C. Figure 9(a) shows a hole (white circle), in the surface carbon that gets filled by mobile Gd atoms by figure 9i. The Gd atoms are likely diffusing from the larger nanoclusters above and across the top of the surface carbon layer (S.I. 3 and S.I. 4). Atomic model schematics of the Gd filling of the hole are shown in figure 9k-m and figure 9n and 9o show the same region before and after filling with Gd atoms. Figure 9o shows that the small cluster is single atom thickness as determined by the ADF-STEM intensity at each atomic position. The 2D lattice of Gd has a periodic arrangement of Gd atoms which are about 0.35 nm ± 0.2 nm apart. The distance within this 2D lattice is larger than that of the known distance of Gd atoms in bulk hcp. The presence of more Gd atoms at one place, which is expected from the drop casting method, also led to the formation of a 3D crystal structure corresponding to a hexagonal close packed arrangement.

The size of the hole in the amorphous carbon in figure 9 is constant, which indicates that Gd atoms do not etch the graphene or the amorphous carbon at the edges, in contrast to previously published work [48]. The increased mobility of Gd atoms at 900°C indicates that this phenomenon happens due to the heating of the sample and is not driven by the electron beam. The Gd atoms only become temporarily localized on the amorphous carbon surface or along the edges and not on the pristine graphene surface, giving rise to step by step hopping and the absence of Gd atoms on pristine graphene regions, which agrees with previously published results [22]. We also observed the pinning of Gd clusters to the edges of the amorphous

surface carbon even after a considerable amount of time (10 min of e-beam exposure) which may indicate that the Gd atoms bonded to the lattice become embedded in the graphene as dopants.

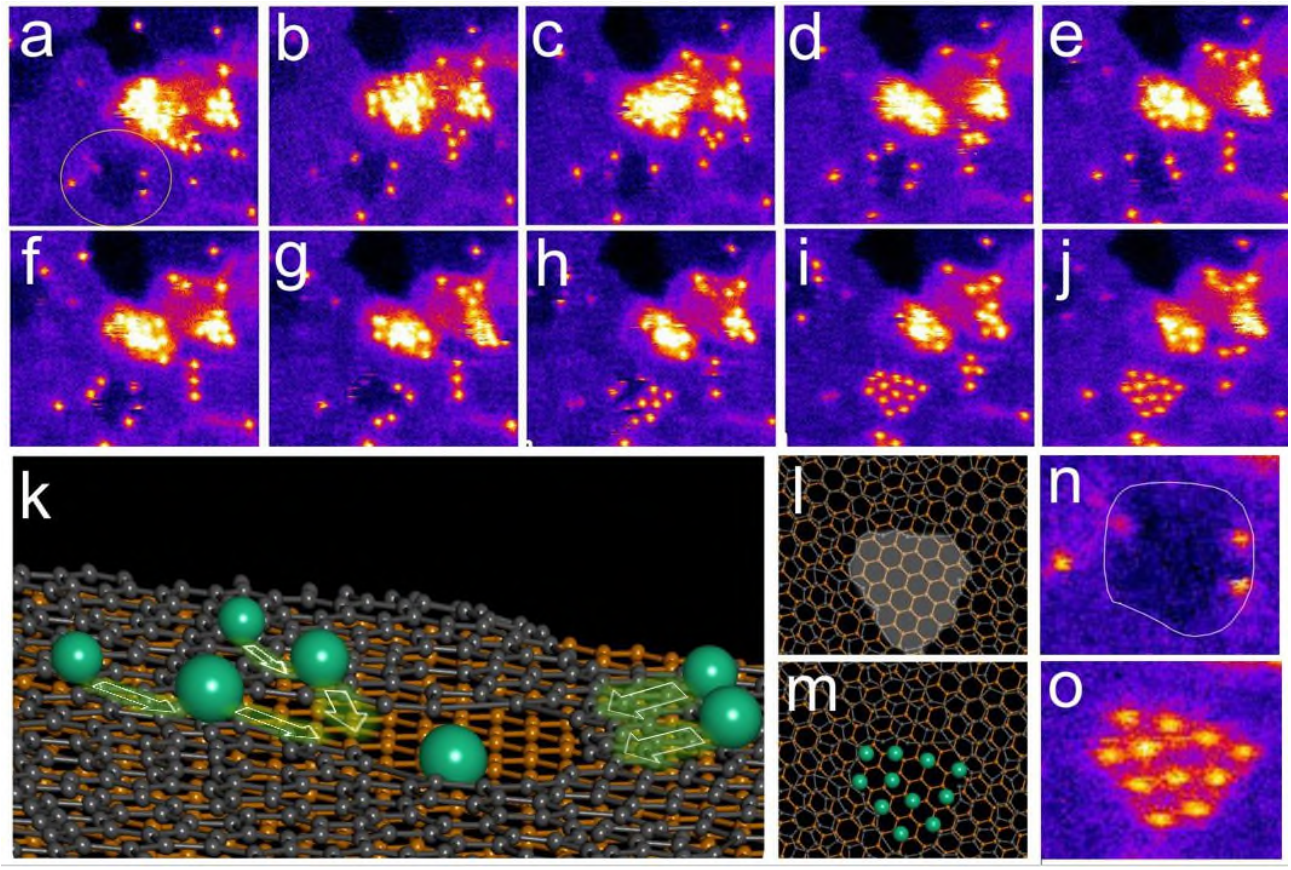

Figure 9. (a)-(j) Time series of ADF-STEM images recorded at 900ºC at an accelerating voltage of 60kV of Gd atoms migrating across the surface of graphene. Colour is used to increase the contrast from Gd atoms. The circle in (a) indicates a void in the surface carbon layer that acts as a sink to trap mobile Gd atoms. Time between frames is ~20s. (k) Schematic atomic model illustrating the migration of Gd atoms into the hole present in the monolayer surface carbon layer that resides on the graphene. (l) Schematic atomic model showing a hole (white shaded area) in top view and (m) after filling with Gd atoms (green). (n) ADF-STEM image of the region indicated by the circle in (a) of the hole and (o) the same area from (j) with Gd filling.

Edge mediated diffusion of Gd atoms also occurs as shown in detail in figure 10, where sequential ADF-STEM images were taken from the same hydrogen annealed graphene:$Gd_3N@C_{80}$ sample examined

in figure 7-9, again measured *in-situ* at 900°C. Annotated images are displayed below each respective ADF-STEM image in figure 10, showing the Gd atoms as yellow spots, the graphene monolayer in orange, the monolayer surface carbon as green and the secondary surface carbon layer as cyan. White lines are marked on figure 10e to indicate the edge regions. Red circles in figure 10e show Gd atoms that remain localized during the imaging. The white arrows are used to indicate the general migration direction of atoms in the frame. In figure 10g, one Gd atom has diffused across the surface carbon layer to be trapped in the central region and remains fairly localized during the subsequent imaging. However, the Gd atoms indicated in figure 10e were generally mobile and end up migrating on the step edge between the graphene and the monolayer surface carbon during the image sequence (figure 10i-l). One by one, Gd atoms migrate around the edge region confirming that the edge mediates a diffusion pathway.

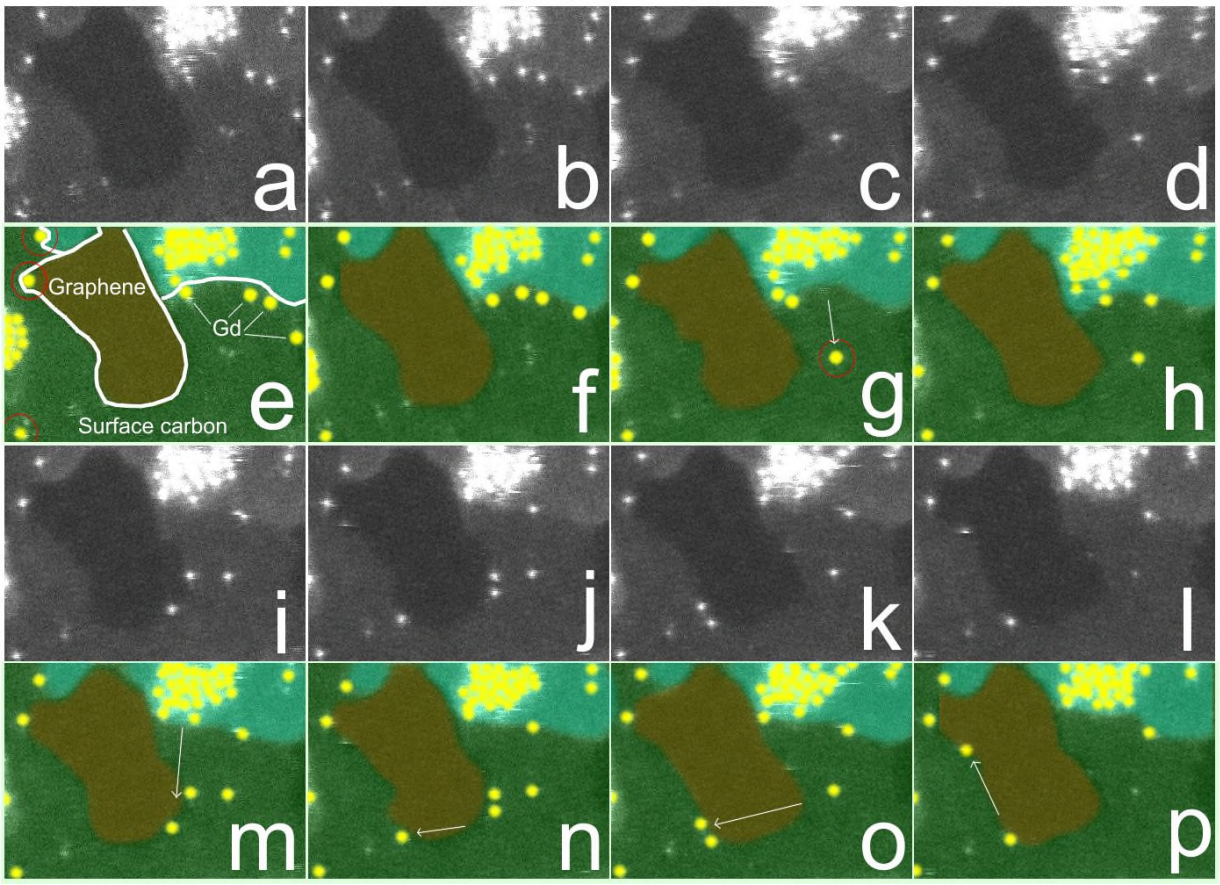

Figure 10. (a)-(d),(i)-(l) Time series of ADF-STEM images taken from a hydrogen annealed graphene:$Gd_3N@C_{80}$ sample with *in-situ* heating at 900ºC showing diffusion of Gd atoms around the edge of the surface carbon regions on graphene. Time between frames is 20s. (e)-(h),(m)-(p). Annotated images from the ADF-STEM images are shown above each, with Gd atoms in yellow, graphene in orange, the green area showing monolayer surface carbon and cyan showing bilayer surface carbon. White arrows indicate the general direction of atom migration. All images were recorded at 60kV.

Finally we have studied the time-dependent cluster-cluster interactions, at the sub-10 atom level (figure 11), in the same samples as in figure 9 and 10 (Hydrogen annealed and *in-situ* at 900ºC). The Gd clusters in figure 11 reside on top of the surface carbon layer and yellow circles are used to indicate two small Gd clusters of 5 atoms and one larger of ~17 Gd atoms in figure 11a. The larger cluster then splits into three smaller ones in figure 11b, reassembles back into a larger linear cluster (figure 11c), before splitting up again into three smaller clusters as shown in figure 11d. The two smaller clusters from figure 11a remain fairly constant in size and structure during this process. The small clusters of ~5 Gd atoms typically have Gd-Gd distances of 0.35nm, similar to those in figure 9o and adopt similar in-plane arrangements. From figure 11d-f, the three small clusters that came from the fragmentation of the larger cluster in figure 11c, remain separated before recombining as shown in figure 11g, and remain in this configuration in figure 11h. These time series of images show that small Gd clusters of ~5 atoms are relatively stable and rapidly fragment from bigger clusters on the surface carbon layer at high temperatures of 900ºC, and do not aggregate into larger nanoclusters. Although the cluster fragmentation is slower at lower temperature, they still show energetically more stable states in 2D space instead of 3D clusters. The surface carbon layer is known to be highly defective and is thus likely to offer multiple binding sites to stabilize the Gd atoms and reduce their migration.

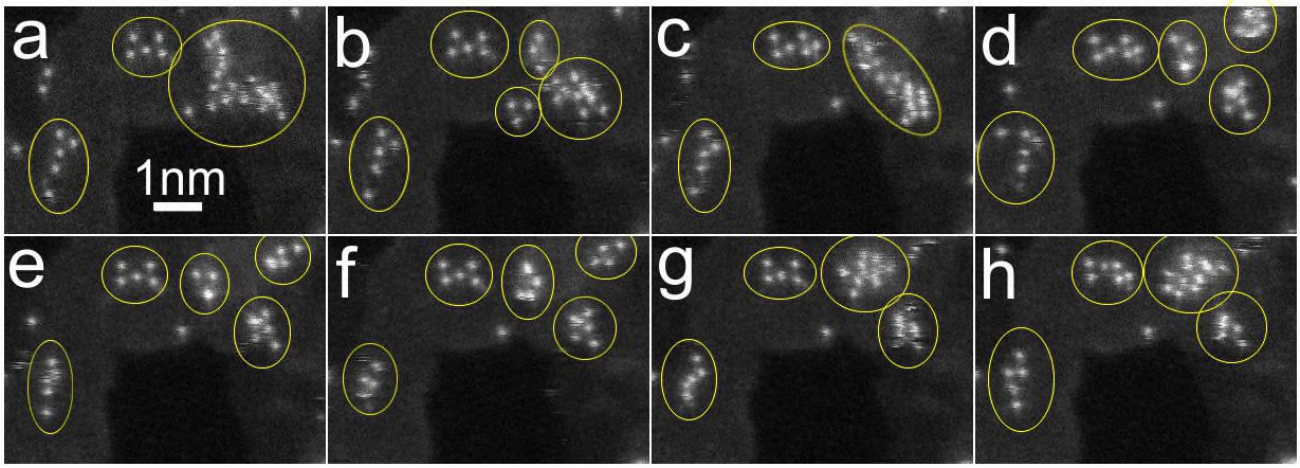

Figure 11. (a)-(h) Time series of ADF-STEM images taken from a hydrogen annealed graphene:$Gd_3N@C_{80}$ sample with *in-situ* heating to 900ºC. Time between images is 20s. Yellow ovals indicate clusters.

Conclusion

The results described reveal how single rare earth metal atom dopants can be delivered to the surface region of 2D materials, with good dispersion and stability up to temperatures reaching 900ºC in vacuum using a molecular precursor deposited from solution. The molecular precursor was in the form of an endohedral metallofullerene. ADF-STEM images revealed the atomic level structure and dynamics of Gd atoms during their temperature dependent transformation. The surface carbon layer on graphene played an important role to first provide anchor sites for MFs to bind before they sublime from the graphene surface. We have showed that the fullerene cage first attaches to the surface carbon before opening up and releasing the Gd atoms. The surface carbon then provides the framework for Gd diffusion across the top and also around its edges, enabling Gd atoms to assemble into small clusters. Gd clusters of 5 atoms were stable at temperatures up to 900ºC, and migrating Gd atoms were found to assembly in voids within the surface carbon and form 2D monolayer crystals with a closed-packed structure. Hydrogen annealing at low temperatures has been demonstrated to be an effective way to achieve high Gd loading onto graphene surfaces. Prolonged exposure of hydrogen to the $Gd_3N@C_{80}$ – graphene system enables fragmentation of

the cages without exposing the sample to very high temperatures. Empty fullerene-like cages were found attached to the surface carbon region at various temperatures, which eventually fused into the surface carbon layer to expand its area. These results provide a pathway to realizing a wide range of rare earth dopants on graphene surfaces. Furthermore, a degree of control on dopant levels and structures can be achieved *via* a combination of *in situ* heating and hydrogen annealing. This can be important for several applications of graphene, including spintronics and catalysis, especially taking into account the dozens of different types of endohedral metallofullerenes that are available from work over the past couple of decades, and can contain encapsulated single-, double- or tri - rare earth heavy metals. Gadolinium based molecules still remain the one of the most important contrast agents for magnetic resonance (MRI) imaging. In this case, our method can potentially be used for drug delivery and imagine where graphene can act as a host to introduce the Gd atoms. The opening of MFs causes cargo release of dopant adatoms on the graphene surface without chemically etching of the underlying graphene or damaging the sample itself, providing an excellent way to create doped graphene monolayers.

Experimental Methods

Chemical vapour deposition growth of graphene

Graphene was synthesized by chemical vapor deposition (CVD) on a copper substrate. A piece of copper foil was first sonicated in a diluted hydrochloric acid solution (HCl, 1 mol/L) to remove the oxides on the copper surface. The copper foil was then sonicated in DI water, acetone and isopropanol (IPA) for 5 min each to remove organic residues. To ensure uniformity of temperature during the whole growth process, the copper foil was positioned in the center of a furnace. 1% methane in argon (CH_4), 25% hydrogen in argon (H_2), and 100% argon (Ar) were used for graphene synthesis. Before the reaction started, the system was first purged with 1000 sccm Ar, 500 sccm H_2, and 100 sccm CH_4 for 30 min. The

furnace was then heated to 1060 °C with a ramp rate of 50 °C/min accompanied by a flow of 500 sccm Ar and 100 sccm H_2. When the temperature reached 1060 °C, the copper was then annealed with the same flow rate for 1 hour. Following the annealing process, the synthesis was carried out at 1060 °C for 1 hr with a flow of 500 sccm Ar, 100 sccm H_2, and 5 sccm CH_4. The furnace was removed from the sample, which allowed the sample to be fast cooled to room temperature.

Metallofullerene

$Gd_3N@C_{80}$ (97% purity) was purchased from S.E.S. research and further purified *via* high performance liquid chromatography (HPLC) (toluene eluent, 16 ml/min, Buckyprep-M column, 20x250 mm). The mass spectra can found in S.I. 4.

TEM sample preparation

Graphene was transferred onto a TEM chip for a DENS SiN *in-situ* heating holder using a PMMA support. It was cleaned by Ar/H_2 and vacuum annealing.

1mg/ml concentration of the solution of the MF in Carbon Disulfide (CS_2) was used to drop cast on the graphene and the TEM holder was baked in vacuum at 60 ºC to remove all the solvents from the surface. One sample was imaged as it was after vacuum baking and other one was H_2 annealed at 180 ºC overnight.

Electron Microscopy

In-situ ADF-STEM imaging was carried using an aberration-corrected JEOL ARM300CF STEM equipped with a JEOL ETA corrector operated under an accelerating voltage of 60 kV located in the electron Physical Sciences Imaging Centre (ePSIC) at Diamond Light Source. Dwell times of 5−20 μs and a pixel size of 0.006 nm px^{-1} were used for imaging. A CL aperture of 30 μm, convergence semi-angle of 31.5 mrad, beam current of 44 pA, and inner acquisition angle of 49.5−198 mrad. Room temperature ADF-STEM imaging was performed using a JEOL ARM200F at 200kV located at the David Cockayne Centre for Electron Microscopy (DCCEM) within the Department of Materials at the University

of Oxford. Imaging conditions used a 30 μm CL aperture with a convergence semi-angle of 22.5 mrad and a beam current of 35pA. The acquisition angles for these images was 72.8 – 271 mrad.

In-situ high-temperature imaging up to 900 °C was performed using a commercially available heating holder from DENS Solutions (SH30-4M-FS). Heating the sample was achieved by passing a current through a platinum resistive coil embedded in the TEM chip (DENS Solutions DENS-C-30). The resistance of the platinum coil was monitored in a four-point configuration, and the temperature was calculated using the Callendar-Van Dusen equation (with calibration constants provided by the manufacturer). Slits were produced in the Si_3N_4 membranes using focused ion beam milling before transferring the graphene.

Images were processed using the ImageJ software. Atomic models were constructed using Accelrys Discovery Studio Visualizer. Multislice image simulations were performed using JEMS with conditions that corresponding to the experimental conditions: chromatic aberration at 60 kV =0.89 mm; spherical aberration = 5μm; energy spread = 0.42eV; probe size =65pm and the convergence semi angle =31.5mrad. The angular range for dark field imaging was between 49.5mrad to 198mrad.

Supporting Information

The Supporting Information is available free of charge on the ACS Publications website. Extra ADF-STEM images showing $Gd_3N@C_{80}$ fusion with surface carbon and Gd metal release, migration of single Gd atoms, and mass spectroscopy of MFs.

Acknowledgements

J.H.W. thanks the support from the Royal Society and an ERC Consolidator Grant (LATO 725258). SS thanks the joint committee of Linacre College and MPLS division of the University of Oxford for financial support through the Women in Science Scholarship and EPSRC studentship. KP acknowledges EPSRC

for support (EP/K030108/1). The Authors acknowledge use of characterization facilities within the David Cockayne Centre for Electron Microscopy at the Department of Materials, University of Oxford.

References

(1) Hong, H.-K.; Jo, J.; Hwang, D.; Lee, J.; Kim, N. Y.; Son, S.; Kim, J. H.; Jin, M.-J.; Jun, Y. C.; Erni, R.; Kwak, S. K.; Yoo, J-W.; Lee, Z.; Atomic Scale Study on Growth and Heteroepitaxy of ZnO Monolayer on Graphene. *Nano Lett.* **2017**, *17*, 120–127.

(2) Kim, H.; Lien, D. H.; Amani, M.; Ager, J. W.; Javey, A. Highly Stable Near-Unity Photoluminescence Yield in Monolayer MoS_2 by Fluoropolymer Encapsulation and Superacid Treatment. *ACS Nano* **2017**, *11*, 5179–5185.

(3) Gan, L. Y.; Zhang, Q.; Cheng, Y.; Schwingenschlögl, U. Photovoltaic Heterojunctions of Fullerenes with MoS_2 and WS_2 Monolayers. *J. Phys. Chem. Lett.* **2014**, *5*, 1445–1449.

(4) Luo, C. Y.; Huang, W. Q.; Xu, L.; Yang, Y. C.; Li, X.; Hu, W.; Peng, P.; Huang, G. F. Electronic Properties and Photoactivity of Monolayer MoS_2/Fullerene van Der Waals Heterostructures. *RSC Adv.* **2016**, *6*, 43228–43236.

(5) Liu, X.; Wang, C.-Z.; Hupalo, M.; Lin, H.-Q.; Ho, K.-M.; Tringides, M. Metals on Graphene: Interactions, Growth Morphology, and Thermal Stability. *Crystals* **2013**, *3*, 79–111.

(6) Hemasiri, B. W. N. H.; Kim, J. K.; Lee, J. M. Synthesis and Characterization of Graphene/ITO Nanoparticle Hybrid Transparent Conducting Electrode. *Nano-Micro Lett.* **2018**, *10*, 1–12.

(7) Maddi, C.; Bourquard, F.; Barnier, V.; Avila, J.; Asensio, M. C.; Tite, T.; Donnet, C.; Garrelie, F. Nano-Architecture of Nitrogen-Doped Graphene Films Synthesized from a Solid CN Source. *Sci. Rep.* **2018**, *8*, 1–13.

(8) Wei, D.; Liu, Y.; Wang, Y.; Zhang, H.; Huang, L.; Yu, G.; Synthesis of N-Doped Graphene by Chemical Vapor Deposition and Its Electrical Properties. *Nano Lett.* **2009**, *9*, 1752–1758.

(9) Luo, Z.; Lim, S.; Tian, Z.; Shang, J.; Lai, L.; MacDonald, B.; Fu, C.; Shen, Z.; Yu, T.; Lin, J. Pyridinic N Doped Graphene: Synthesis, Electronic Structure, and Electrocatalytic Property. *J. Mater. Chem.* **2011**, *21*, 8038–8044.

(10) Pi, K.; McCreary, K. M.; Bao, W.; Han, W.; Chiang, Y. F.; Li, Y.; Tsai, S. W.; Lau, C. N.; Kawakami, R. K. Electronic Doping and Scattering by Transition Metals on Graphene. *Phys. Rev. B* **2009**, *80*, 1–5.

(11) Hwang, J. O.; Park, J. S.; Choi, D. S.; Kim, J. Y.; Lee, S. H.; Lee, K. E.; Kim, Y. H.; Song, M. H.; Yoo, S.; Kim, S. O. Workfunction-Tunable, N-Doped Reduced Graphene Transparent Electrodes for High-Performance Polymer Light-Emitting Diodes. *ACS Nano* **2012**, *6*, 159–167.

(12) Kasry, A.; Kuroda, M.; Martyna, G.; Tulevski, G.; Bol, A. Chemical Doping of Large-Area Stacked Graphene Films for Use as Transparent, Conducting Electrodes. *J. Am. Chem. Soc.* **2010**, *4*, 3839–3844.

(13) Kim, K. S.; Moradian, A.; Mostaghimi, J.; Soucy, G. Modeling of Induction Plasma Process for Fullerene Synthesis: Effect of Plasma Gas Composition and Operating Pressure. *Plasma Chem. Plasma Process.* **2010**, *30*, 91–110.

(14) Liu, H.; Liu, Y.; Zhu, D. Chemical Doping of Graphene. *J. Mater. Chem.* **2011**, *21*, 3335–3345.

(15) Lv, R.; Li, Q.; Botello-Méndez, A. R.; Hayashi, T.; Wang, B.; Berkdemir, A.; Hao, Q.; Eléas, A. L.; Cruz-Silva, R.; Gutiérrez, H. R.;Kim, Y. A.; Muramatsu, H.; Zhu, J.; Endo, M.; Terrones, H.; Charlier, J-C.; Pan, M.; Terrones, M.; Nitrogen-Doped Graphene: Beyond Single Substitution and Enhanced Molecular Sensing. *Sci. Rep.* **2012**, *2*, 1–8.

(16) He, Z.; He, K.; Robertson, A. W.; Kirkland, A. I.; Kim, D.; Ihm, J.; Yoon, E.; Lee, G. D.; Warner, J. H. Atomic Structure and Dynamics of Metal Dopant Pairs in Graphene. *Nano Lett.* **2014**, *14*, 3766–3772.

(17) Tsetseris, L.; Wang, B.; Pantelides, S. T. Substitutional Doping of Graphene: The Role of Carbon Divacancies. *Phys. Rev. B* **2014**, *89*, 3–6.

(18) Deng, X.; Zeng, J.; Si, M.; Lu, W. The Mechanism and Process of Spontaneous Boron Doping in Graphene in the Theoretical Perspective. *Phys. Lett. A.* **2016**, *380*, 3384–3388.

(19) Warner, J. H.; Lin, Y. C.; He, K.; Koshino, M.; Suenaga, K. Stability and Spectroscopy of Single Nitrogen Dopants in Graphene at Elevated Temperatures. *ACS Nano* **2014**, *8*, 11806–11815.

(20) Robertson, A. W.; Montanari, B.; He, K.; Kim, J.; Allen, C. S.; Wu, Y. A.; Olivier, J.; Neethling, J.; Harrison, N.; Kirkland, A. I.; Warner, J. H.; Dynamics of Single Fe Atoms in Graphene Vacancies. *Nano Lett.* **2013**, *13*, 1468–1475.

(21) Liu, X.; Wang, C. Z.; Hupalo, M.; Yao, Y. X.; Tringides, M. C.; Lu, W. C.; Ho, K. M. Adsorption and Growth Morphology of Rare-Earth Metals on Graphene Studied by *Ab Initio* Calculations and Scanning Tunneling Microscopy. *Phys. Rev. B* **2010**, *82*, 1–7.

(22) Chen, Q.; He, K.; Robertson, A. W.; Kirkland, A. I.; Warner, J. H. Atomic Structure and Dynamics of Epitaxial 2D Crystalline Gold on Graphene at Elevated Temperatures. *ACS Nano* **2016**, *10*, 10418–10427.

(23) Gan, Y.; Sun, L.; Banhart, F. One- and Two-Dimensional Diffusion of Metal Atoms in Graphene. *Small* **2008**, *4*, 587–591.

(24) Sloan, J.; Liu, Z.; Suenaga, K.; Wilson, N. R.; Pandey, P. A.; Perkins, L. M.; Rourke, J. P.; Shannon, I. J. Imaging the Structure, Symmetry, and Surface-Inhibited Rotation of Polyoxometalate Ions on Graphene Oxide. *Nano Lett.* **2010**, *10*, 4600–4606.

(25) Bosch-Navarro, C.; Perkins, L. M.; Kashtiban, R. J.; Rourke, J. P.; Shannon, I. J.; Sloan, J. Selective Imaging of Discrete Polyoxometalate Ions on Graphene Oxide under Variable Voltage Conditions. *ACS Nano* **2016**, *10*, 796–802.

(26) Warner, J. H.; Ito, Y.; Zaka, M.; Ge, L.; Akachi, T.; Okimoto, H.; Porfyrakis, K.; Watt, A. A. R.; Shinohara, H.; Briggs, G. A. D. Rotating Fullerene Chains in Carbon Nanopeapods. *Nano Lett.* **2008**, *8*, 2328–2335.

(27) Zhou, W.; Kapetanakis, M. D.; Prange, M. P.; Pantelides, S. T.; Pennycook, S. J.; Idrobo, J. C. Direct Determination of the Chemical Bonding of Individual Impurities in Graphene. *Phys. Rev. Lett.* **2012**, *109*, 2–6.

(28) Zhou, W.; Lee, J.; Nanda, J.; Pantelides, S. T.; Pennycook, S. J.; Idrobo, J. C. Atomically Localized Plasmon Enhancement in Monolayer Graphene. *Nat. Nanotechnol.* **2012**, *7*, 161–165.

(29) Crowe, I. F.; Roschuk, T.; Bangert, U.; Sherliker, B.; Halsall, M. P.; Knights, A.; Mascher, P. Combined Super-STEM Imaging, EEL and PL Spectroscopy of Un-Doped and Er Doped SRSO on Si. *Conf. Optoelectron. Microelectron. Mater. Devices, Proceedings, COMMAD* **2008**, 163–165.

(30) Guo, S.; Wen, D.; Zhai, Y.; Dong, S.; Wang, E. Platinum Nanoparticle Ensemble-on-Graphene Hybrid Nanosheet: One-Pot Rapid Synthesis , and Used as New Electrode Materials for Electrochemical Sensing. *ACS Nano* **2010**, *4*, 3959–3968.

(31) Lin, Y. C.; Teng, P. Y.; Yeh, C. H.; Koshino, M.; Chiu, P. W.; Suenaga, K. Structural and Chemical Dynamics of Pyridinic-Nitrogen Defects in Graphene. *Nano Lett.* **2015**, *15*, 7408–7413.

(32) Wang, S.; Sawada, H.; Han, X.; Zhou, S.; Li, S.; Guo, Z. X.; Kirkland, A. I.; Warner, J. H. Preferential Pt Nanocluster Seeding at Grain Boundary Dislocations in Polycrystalline Monolayer MoS_2. *ACS Nano* **2018**, *12*, 5626-5636

(33) Tsang, S. C.; Chen, Y. K.; Harris, P. J. F.; Green, M. L. H. A Simple Chemical Method of Opening and Filling Carbon Nanotubes. *Nature* **1994**, *372*, 159–162.

(34) Allen, C. S.; Ito, Y.; Robertson, A. W.; Shinohara, H.; Warner, J. H. Two-Dimensional Coalescence Dynamics of Encapsulated Metallofullerenes in Carbon Nanotubes. *ACS Nano* **2011**, *5*, 10084–

10089.

(35) Khlobystov, A. N.; Britz, D. A; Briggs, G. A. D. Molecules in Carbon Nanotubes Molecules in Carbon Nanotubes. *Acc. Chem. Res.* **2005**, *38*, 901–909.

(36) Qin, Z.; Qin, G.; Shao, B.; Zuo, X. Unconventional Magnetic Anisotropy in One-Dimensional Rashba System Realized by Adsorbing Gd Atom on Zigzag Graphene Nanoribbons. *Nanoscale* **2017**, *9*, 11657–11666.

(37) Lu, Y.; Zhou, T. G.; Shao, B.; Zuo, X.; Feng, M. Carrier-Dependent Magnetic Anisotropy of Gd-Adsorbed Graphene. *AIP Adv.* **2016**, *6, 055708*.

(38) Alemani, M.; Barfuss, A.; Geng, B.; Girit, C.; Reisenauer, P.; Crommie, M. F.; Wang, F.; Zettl, A.; Hellman, F. Effect of Gadolinium Adatoms on the Transport Properties of Graphene. *Phys. Rev. B* **2012**, *86*, 1–5.

(39) Talyzin, A. V.; Tsybin, Y. O.; Purcell, J. M.; Schaub, T. M.; Shulga, Y. M.; Noréus, D.; Sato, T.; Dzwilewski, A.; Sundqvist, B.; Marshall, A. G. Reaction of Hydrogen Gas with C60 at Elevated Pressure and Temperature: Hydrogenation and Cage Fragmentation. *J. Phys. Chem. A* **2006**, *110*, 8528–8534.

(40) Cretu, O.; Komsa, H. P.; Lehtinen, O.; Algara-Siller, G.; Kaiser, U.; Suenaga, K.; Krasheninnikov, A. V. Experimental Observation of Boron Nitride Chains. *ACS Nano* **2014**, *8*, 11950–11957.

(41) Warner, J. H.; Rümmeli, M. H.; Ge, L.; Gemming, T.; Montanari, B.; Harrison, N. M.; Büchner, B.; Briggs, G. A. D. Structural Transformations in Graphene Studied with High Spatial and Temporal Resolution. *Nat. Nanotechnol.* **2009**, *4*, 500–504.

(42) Cowley, J. M.; Moodie, A. F. A New Formulation of Scalar Diffraction Theory for Restricted Aperture. *Proc. Phys. Soc.* **1958**, *71*, 533–545.

(43) Stadelmann, P. Image Analysis and Simulation Software in Transmission Electron Microscopy.

Microsc. Microanal. **2003**, *9*, 60–61.

(44) Lu, J.; Sabirianov, R. F.; Mei, W. N.; Gao, Y.; Duan, C.; Zeng, X. Structural and Magnetic Properties of $Gd_3N@C_{80}$. *J. Phys. Chem. B* **2006**, *110*, 23637–23640.

(45) Krause, M.; Dunsch, L. Gadolinium Nitride Gd3N in Carbon Cages: The Influence of Cluster Size and Bond Strength. *Angew. Chemie - Int. Ed.* **2005**, *44*, 1557–1560.

(46) Mirzayev, R.; Mustonen, K.; Monazam, M. R. A.; Mittelberger, A.; Pennycook, T. J.; Mangler, C.; Susi, T.; Kotakoski, J.; Meyer, J. C. Buckyball Sandwiches. *Sci. Adv.* **2017**, *3*, e1700176.

(47) Stevenson, S.; Phillips, J. P.; Reid, J. E.; Olmstead, M. M.; Rath, P.; Balch, A. L. Pyramidalization of Gd_3N inside a C80 Cage . The Synthesis and Structure of $Gd_3N@C_{80}$. **2004**, 2814–2815.

(48) Tsukamoto, T.; Ogino, T. Control of Graphene Etching by Atomic Structures of the Supporting Substrate Surfaces. *J. Phys. Chem. C* **2011**, *115*, 8580–8585.

TOC graphic